

■ Boron(III) Chelates

Synthesis, Structure and Photophysical Properties of a New Class of Inherently Chiral Boron(III) Chelates—The *tert*-Leucine ComplexesNawaf Algoazy,^[a] Julian G. Knight,^{*,[a]} Paul G. Waddell,^[b] Roy Aerts,^[c] Wouter Herrebout,^{*,[c]} Hatun H. T. Al-Sharif,^[d] Joshua K. G. Karlsson,^[d] and Anthony Harriman^{*,[d]}

Abstract: A new family of boron(III) chelates is introduced whereby molecular chirality, confirmed by circular dichroism, is imported during synthesis such that isolation of the diastereoisomers does not require separation procedures. The photophysical properties of two members of the family have been examined: the *N,O,O*-salicylaldehyde-based derivative shows pronounced intramolecular charge-transfer character in fluid solution and is weakly fluorescent, with a large Stokes shift. The corresponding 2-methylamino-benzaldehyde-derived *N,N,O*-chelate absorbs and fluoresces in the

visible region with a much smaller Stokes shift. Orange fluorescence is also observed for this compound as a cast film. Temperature-dependence studies show that decay of the fluorescent state is weakly activated but emission is less than quantitative at 77 K. Quite rare for boron(III)-based chelates, this derivative undergoes intersystem crossing to form a meta-stable triplet-excited state. X-ray crystal structures are reported for both compounds, along with simulated ECD spectra.

Introduction

Numerous disparate types of boron-containing fluorophores have emerged over recent years.^[1] Many of these attractive molecular modules derive from the well-known boron dipyrromethene (BODIPY)^[2,3] family of dyes. In fact, the BODIPY chromophore is sufficiently versatile in terms of structural amenability that in excess of a thousand derivatives are now known.^[4,5] Much of the interest in these compounds relates to

the opportunity to shift the absorption and emission maxima towards lower energies without compromising on emission luminosity. For example, the so-called aza-BODIPY dyes retain similar structures to the corresponding BODIPY parent but the absorption maxima are red shifted by ca. 100 nm or more.^[6] Other important classes of related boron-based fluorophores include the BOPHY (i.e., *bis*(difluoroboron)-1,2-*bis*((1H-pyrrol-2-yl)methylene)hydrazine)^[7,8] and BORANIL (i.e., B(III) complexes of substituted anils)^[9] families. The BOPHY system, in particular, offers a symmetrical scaffold displaying high fluorescence quantum yields and excellent levels of photostability.^[10] These compounds are readily functionalised to provide a wide range of optical band gaps. The main strengths of the BORANIL compounds concern their facile synthesis and their relatively strong emission in the crystalline state.^[11] Of course, there are several other classes of fluorescent molecules where a tetrahedral boron(III) centre is used to arrange the ligand into a “rigid” macrocycle.^[12] In so doing, it becomes possible to introduce molecular chirality by appropriate substitution but, in the vast majority of cases, the enantiomers have to be isolated by rather tedious separation procedures.^[13] The resultant materials can be analysed by circular dichroism and, in certain systems, give rise to circularly polarised luminescence.^[13,14] The latter signature is significant in terms of potential development of novel 3D optical display, storage or processing systems.^[15] There is additional interest in identifying enantio-selective luminescent sensors that might provide unparalleled recognition capabilities for key bio-molecules *in situ*.^[16]

Expanding the search for new fluorescent reagents, our attention was drawn to the benzo-oxazaborolo-oxazaboroni-

[a] N. Algoazy, Dr. J. G. Knight
School of Natural and Environmental Sciences, Bedson Building
Newcastle University
Newcastle upon Tyne, NE1 7RU (UK)
E-mail: J.G.Knight@ncl.ac.uk

[b] Dr. P. G. Waddell
Crystallography Laboratory
School of Natural and Environmental Sciences, Bedson Building
Newcastle University
Newcastle upon Tyne, NE1 7RU (UK)

[c] Dr. R. Aerts, Dr. W. Herrebout
Department of Chemistry
University of Antwerp
Groenenborgerlaan 171, 2020 Antwerp (Belgium)
E-mail: wouter.herrebout@uantwerpen.be

[d] Dr. H. H. T. Al-Sharif, Dr. J. K. G. Karlsson, Prof. Dr. A. Harriman
Molecular Photonics Laboratory
School of Natural and Environmental Sciences, Bedson Building
Newcastle University
Newcastle upon Tyne, NE1 7RU (UK)
E-mail: anthony.harriman@ncl.ac.uk

Supporting information and the ORCID identification numbers for the authors of this article can be found under:
<https://doi.org/10.1002/chem.202005246>

nones. These particular compounds feature a heterocyclic ring system containing a boron(III) centre and were first described by Vedejs^[17] in the context of crystallization-induced asymmetric transformations and also by Hutton^[18] as the product of tautomerisation to form a chiral chelate stereogenic only at the boron atom. Gois^[19] subsequently reported a one-pot synthesis of these boron chelates from a salicylaldehyde, aryl boronic acid and α -amino acid under aqueous conditions and has investigated their use as enzyme inhibitors. To date, there has been no report of the photophysical properties of this heterocyclic system.

Because of the strong appeal of chiral fluorophores as potential selective bio-labels,^[15,16,20] we have further developed this range of boron(III)-containing chelates to include the previously unreported *tertiary*-leucine-derived ligand. The inclusion of the sterically bulky *tertiary*-butyl group was designed to: (a) increase the differentiation between the faces of the bicyclic chelate and thus the diastereo-control during formation of the stereogenic centre at boron; (b) result in greater restriction of conformational freedom, such as the rotation of the aryl substituent on the boron atom, thus potentially reducing pathways for nonradiative decay; (c) provide increased steric protection against nucleophilic attack at the imine-like carbon, known to be involved in the hydrolysis of the heterocycle,^[21] and (d) hinder deprotonation α -to the carbonyl group which presents a potential route to racemization during the condensation reaction. In addition to the salicylaldehyde-derived *N,O,O*-chelate, and in order to explore the influence of the composition of the heterobicyclic ring on the optical properties, we have prepared the corresponding 2-methylamino-benzaldehyde-derived *N,N,O*-chelate, which represents a new heterobicyclic ring system. These compounds are synthesized in a one-pot procedure that does not require elaborate purification procedures but favours simple adaptation to include different heteroatoms in the molecular framework.

Since the *tert*-leucine group can be optically resolved prior to synthesis, the resultant compounds are inherently chiral and do not racemise during the condensation stage. This avoids the need for isolation of the enantiomers from a racemic mix-

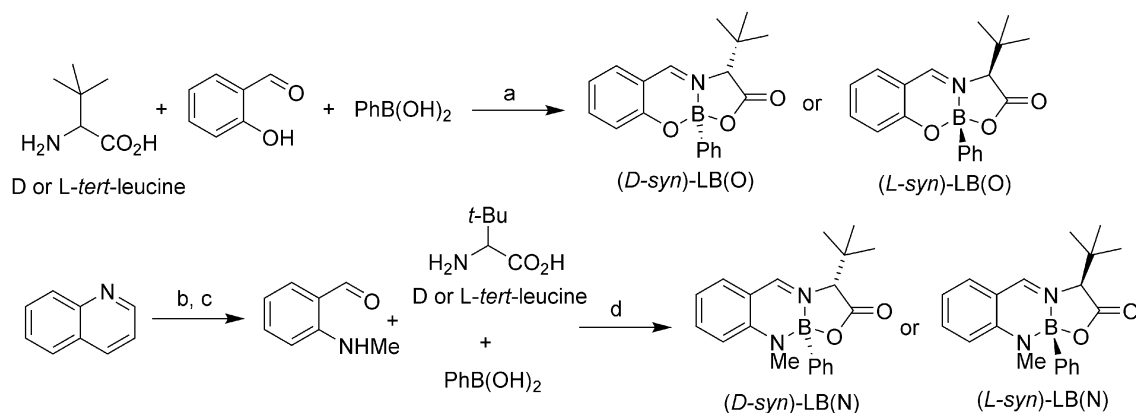
ture, provided the starting material is optically pure. We now describe the synthesis and selected optical properties of two representative derivatives of this new family. It will be shown that the photophysical properties are sensitive to the composition of the heterobicyclic ring formed around the boron(III) centre.

Results and Discussion

Synthesis and structural characterisation

The enantiomeric salicylaldehyde-derived boron(III) chelates, hereafter termed *tert*-leucine-complexes and abbreviated as LB(O), were prepared by the two-step, one-pot condensation of *D*- or *L*-*tert*-leucine with salicylaldehyde under aqueous conditions. Formation of the intermediate Schiff's base was followed by addition of phenylboronic acid (Scheme 1). The resultant complexes precipitate from the reaction mixture and were isolated in excellent yield as single diastereoisomers. 2-Dimethylamino-benzaldehyde was prepared from quinoline by the known^[22] sequence of *N*-methylation using iodomethane followed by oxidative cleavage using basic hydrogen peroxide (Scheme 1). The corresponding *N,N,O*-chelates, LB(N), were formed in a single step on heating a mixture of the aldehyde with *tert*-leucine and phenylboronic acid in toluene. The complexes were isolated as single diastereoisomers by column chromatography.

X-ray structural determinations from single crystals of the two compounds indicate a *syn* geometry around the B₁-N₁-C₁₄ fragment, as can be seen in Figure 1; specifically, this means that both the B-phenyl and the C-*tert*-butyl groups point either above or below the plane defined by the heterobicycle. The same geometrical feature is apparent from DFT computational studies^[23] made using the B3LYP functional^[24] and the 6.311 + G(d) basis set^[25] with the PCM(CHCl₃) solvent model and Menzucchi–Tomasi correction.^[26] The corresponding *anti* geometry is less favourable by ca. 30 kJ mol⁻¹ for LB(O) and ca. 16 kJ mol⁻¹ for LB(N). Importantly, NMR spectra are consistent with a single species being present in solution such that interconversion be-



Scheme 1. Synthesis of *tert*-leucine complexes LB(O) and LB(N). Reagents: (a) *tert*-leucine, salicylaldehyde, H₂O, 90 °C, 1 h; PhB(OH)₂, 90 °C, 20 h [*D*-*syn*-LB(O) 97%; *L*-*syn*-LB(O) 97%]; (b) quinoline, Mel, toluene, reflux, 24 h (92%); (c) KOH, 35% H₂O₂, 1,2-DCE/H₂O, 0 °C to rt, 48 h (87%); (d) *tert*-leucine, 2-methylaminobenzaldehyde, PhB(OH)₂, toluene, 90 °C, 24 h [*D*-*syn*-LB(N) 74%; *L*-*syn*-LB(N) 81%].

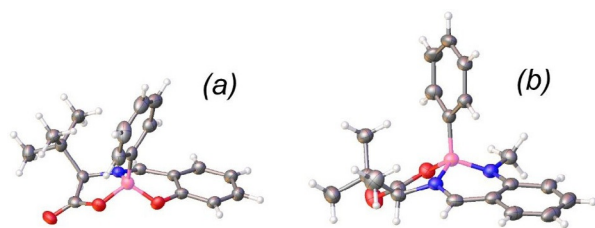


Figure 1. Single-crystal X-ray structures derived for (a) *D*-syn-LB(O) and (b) *L*-syn-LB(N) emphasizing the *syn* relative stereochemistry: ellipsoids were drawn to the 50% probability level.

tween the *syn*- and *anti*-forms does not take place at ambient temperature.

Listed in Table 1 are some of the relevant geometrical features determined from the crystal structures, including key bond lengths and angles (see Figures S12 and S13 for the atom numbering system). In both cases, the boron centre exists as a distorted tetrahedron while the carbonyl group has a bond length of around 1.21 Å, which is quite normal for the C=O bond.^[27] In fact, the close comparability of lactone C=O bond lengths for the two compounds can be used to argue that the molecular polarity around this fragment is closely comparable in both LB(O) and LB(N), at least in the solid state (N.B., increased polarity serves to lengthen the bond). The bond length for the B-phenyl connection is increased for LB(N) and there are accompanying changes in length of the B₁-N₁ and B₁-O₁ bonds. It is noticeable that the boron atom is markedly displaced from the plane defined by the heterobicycle for both LB(O) and LB(N) (Table 1).

The way in which molecules pack in the 3D crystal structure of LB(O) shows that individual molecules form “columns” along the crystallographic [100] direction in which the boron atoms are separated by ca. 6.8 Å (Figure S15). Each molecule is related to the next by pure translational symmetry. The heterobicyclic ring and the phenyl ring are oriented almost perpendicular to each other so as to form a crude “L-shaped” entity with the *tert*-butyl fragment blocking access to one face of the phenyl

ring. These *pseudo*-columns align so that the phenyl ring appears to be orientated towards the centre of the L-shaped species of an adjacent column (Figure S15). The shortest distance between boron atoms associated with adjacent columns is ca. 7.9 Å. The arrangement of molecules into ordered columns is also evident for LB(N) along the crystallographic [100] direction, with neighbouring boron atoms being ca. 7.9 Å apart (Figure S16). However, the orientation of the molecules in each column, and the way in which these columns pack together, differ from those outlined for LB(O). Two structural features can be recognised: firstly, columns assemble such that the lactone groups are directed towards the *tert*-butyl groups of an adjacent column. This motif is seen also for LB(O). Secondly, the ancillary phenyl rings from one column sit close to the rim of the heterobicyclic ring so as to isolate the lactone groups. For LB(N), the shortest B-B distance between neighbouring columns is ca. 7.2 Å (Figure S16).

Computational studies (DFT/B3LYP/6.311+G(d)/PCM(CHCl₃)) are fully consistent with a distorted tetrahedral geometry around the boron centre. Structural information^[23] is provided as part of the Supporting Information and important parameters are given in Table 1. The computational studies allow calculation of the molecular dipole moments^[28] as being 8.8 D and 6.2 D, respectively, for LB(O) and LB(N), while the transition dipole length is ca. 7.6 Å. The direction of the dipole vector is indicated by way of Figures S18 and S23 and, to a crude approximation, runs from the boron(III) centre parallel to the heterobicycle. These computational studies also allow estimation of the energy barrier for rotation of the ancillary phenyl ring around the connecting B₁-C₈ bond. In the absence of concerted structural changes, the projected barriers exceed 100 kJ mol⁻¹ and thereby indicate that full rotation is blocked. Nonetheless, the phenyl ring can gyrate over a variance of ca. 100°. For the energy-minimized geometries, the dihedral angle subtended at the B₁-N₁-C₁₄-C₁₅ connection is -42.2° and -36.0°, respectively, for LB(O) and LB(N) (see Figures S17 and S22.).

Redox properties

Cyclic voltammetry carried out with LB(O) in CH₂Cl₂ containing tetra-*N*-butylammonium tetrafluoroborate (0.2 M) as background electrolyte showed only electrochemically irreversible peaks. On reductive scans (0.06 V s⁻¹), an irreversible, one-electron wave was observed at a peak potential of -1.73 V vs. Ag/Ag⁺. An irreversible, two-electron oxidation process was found on oxidative scans at a peak potential of 1.62 V vs. Ag/Ag⁺. A second oxidation step occurs with a peak potential of 1.89 V vs. Ag/Ag⁺. The difference between the oxidation and reduction peak potentials is 3.33 eV, which is remarkably close to the optical bandgap of 3.35 eV as found in cyclohexane (see later). Note that the irreversible nature of these electrochemical steps, which was unchanged at much higher (i.e., 0.4 V s⁻¹) scan rates, might overestimate the difference between oxidation and reduction processes.^[29]

Kohn-Sham representations of the frontier molecular orbitals^[30] calculated for LB(O) indicate that the LUMO ($E_L =$

Table 1. Salient geometric parameters derived by single-crystal X-ray crystallography and equivalent values as obtained from quantum chemical calculations in a reservoir of CHCl ₃ molecules. ^[a]				
Parameter	LB(O) ^[b]	LB(O)-DFT ^[c]	LB(N) ^[b]	LB(N)-DFT ^[c]
C ₁₅ =O ₂ [Å]	1.213(3)	1.203	1.210(3)	1.203
B ₁ -N ₁ [Å]	1.578(3)	1.593	1.561(3)	1.578
B ₁ -O ₁ [Å]	1.497(3)	1.495	1.509(3)	1.554
B ₁ -N ₂ [Å]			1.525(3)	1.612
B ₁ -C ₈ [Å]	1.599(3)	1.604	1.612(3)	1.484
B ₁ -O ₃ [Å]	1.468(3)	1.481		
O ₁ -B ₁ -O ₂ [°]	109.88(17)	109.23		
N ₂ -B ₁ -O ₁ [°]			113.32(17)	110.87
N ₁ -B ₁ -C ₈ [°]	115.26(17)	116.17	116.51(17)	117.08
Displacement [Å] ^[d]	0.744(3)		0.735(3)	

[a] See Figures S12 and S13 for the atom numbering system used here.
 [b] Data derived from X-ray crystallography. [c] Results from DFT calculations. [d] Displacement of the boron atom from the plane defined by all the atoms forming rings that include the boron atom (see Figure S14).

−2.74 eV) is distributed around the annulated benzene ring, but not involving the C₅ atom, with an important contribution from the N₁ atom (Figure 2). The heterobicyclic O₁ atom makes only a minor contribution towards the LUMO. It is notable that neither the lactone group nor the appended phenyl ring are involved in constructing the LUMO. The latter is separated in energy terms from LUMO(1) ($E_{L1} = -1.46$ eV), a finding that appears consistent with the one-electron reduction wave seen in the cyclic voltammogram. In contrast, the HOMO ($E_H = -6.23$ eV) lies close in energy to both HOMO(−1) ($E_{H1} = -6.53$ eV) and HOMO(−2) ($E_{H2} = -6.64$ eV). This near isoenergetic spacing of the HOMOs might contribute towards the multi-electron oxidation pattern seen in the cyclic voltammogram. The HOMO is concentrated mostly on the annulated benzene ring, not involving the C₃ atom, with an important contribution from the O₁ atom (Figure 2). Unlike the LUMO,

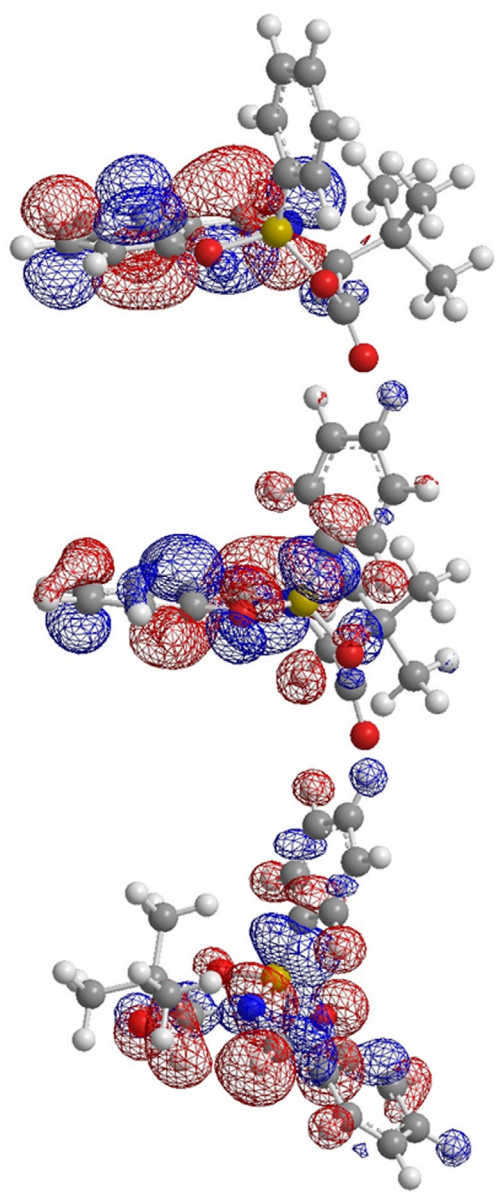


Figure 2. Kohn–Sham orbital representations computed for LB(O), running from top to bottom for LUMO, HOMO and HOMO(−1).

there is only a minor contribution from the N₁ atom but some slight involvement of the appended benzene ring. More importantly, the lactone group plays an important role in defining the HOMO and it is this realisation that leads to the intramolecular charge-transfer character observed^[31] for LB(O). The relative contribution of the lactone group becomes more significant on moving from the HOMO to HOMO(−1) and then HOMO(−2) (Figure 2).

With LB(N), an irreversible reduction step occurs with a peak potential of −1.69 V vs. Ag/Ag⁺. This is closely comparable to the reductive process observed with LB(O) under the same conditions. On oxidative scans there is an irreversible process with a peak potential of 0.89 V vs. Ag/Ag⁺. At more positive potentials, a second wave is seen with a peak potential of 1.57 V vs. Ag/Ag⁺ at a scan rate of 0.06 V s^{−1}. This latter wave is electrochemically irreversible and corresponds to the loss of two electrons.^[29] For LB(N), the potential difference between electrochemical oxidation and reduction steps corresponds to 2.58 eV, which can be compared to the optical band gap of 2.53 eV (see later). It is notable that this compound is significantly easier to oxidise than is LB(O), although all processes are electrochemically irreversible.

Molecular orbital calculations made for LB(N) indicate that the charge distribution for the LUMO is comparable for that of LB(O) (Figure 3). The principal contributor to the LUMO ($E_L = -2.71$ eV) is the heterobicyclic ring, not counting the boron(III) or the N atoms (Figure 3). The lactone group, the C₃ atom and the appended phenyl ring do not contribute significantly to the composition of the LUMO. That the two compounds exhibit comparable reductive electrochemistry, therefore, is not too surprising. The HOMO is also centred on the heterobicycle but involves partial offload of the charge distribution to the phenyl ring. Moreover, the HOMO ($E_H = -5.23$ eV) is separated in energy terms from the HOMO(−1) ($E_{H1} = -6.18$ eV) and HOMO(−2) ($E_{H2} = -6.63$ eV). For these latter molecular orbitals, the lactone makes an important contribution to the overall composition. It is now clear that the main consequence of replacing the oxygen atom with the N(CH₃) group is a significant raising of the HOMO energy. This, in turn, affects the band gap and the ionisation potential.

Photophysical properties of LB(O)

The absorption spectrum recorded for LB(O) in 2-methyltetrahydrofuran (MTHF) solution shows a featureless, symmetrical band centred at ca. 390 nm (Figure 4). This absorption band bears the characteristic hallmarks of an intramolecular charge-transfer transition.^[31] Closely comparable spectral profiles are found in toluene ($\lambda_{\text{ABS}} = 396$ nm) and cyclohexane ($\lambda_{\text{ABS}} = 370$ nm); see Table S5 for a listing of band maxima. Gaussian profile analysis^[32] of the reduced absorption spectrum indicates that the most robust fitting pattern splits the lowest-energy absorption transition into a progression of four closely-spaced components (Figure 4a). This pattern, which is not a unique solution, gives the simplest representation that accurately reproduces the entire absorption envelope in all three solvents. A common full-width at half-maximum (FWHM) can be used

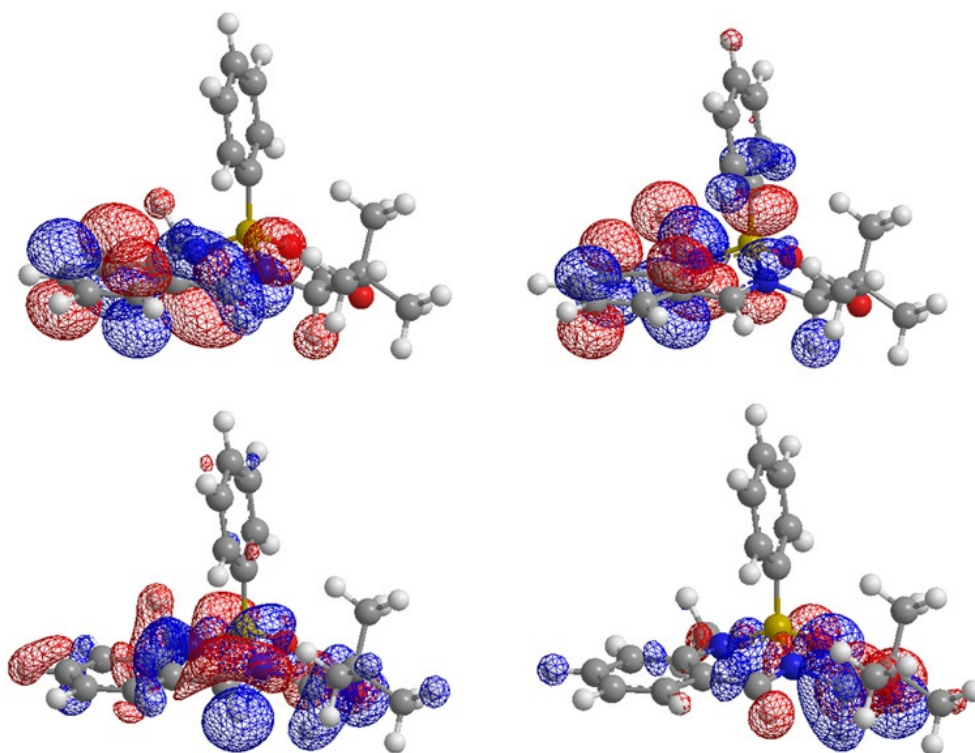


Figure 3. Kohn–Sham orbital representations computed for LB(N); LUMO (top left), HOMO (top right), HOMO(−1) (bottom left), HOMO(−2) (bottom right).

for each solvent and the main fitting parameters are collected in Table S6, where it can be seen that the nature of the solvent has only moderate effect. The underlying vibronic mode coupled to the absorption transition has a value of ca. 1650 cm^{-1} and, as such, might contain an important contribution from an imine stretching vibration.^[33] At higher energies, an additional intramolecular charge-transfer transition can be seen, with a maximum at ca. $33\,300\text{ cm}^{-1}$. The lowest energy absorption band is primarily of HOMO–LUMO character.

On the basis of the Gaussian fitting pattern, the peak of the lowest-energy absorption transition is located as $25\,025\text{ cm}^{-1}$ (i.e., 400 nm) in MTHF solution. The molar absorption coefficient (ϵ_{MAX}) at the band maximum in CHCl_3 was found to be $12\,900\text{ M}^{-1}\text{ cm}^{-1}$, corresponding to an oscillator strength of 0.22. The small solvent effect noted above suggests that the molecule is only marginally stabilised by the surrounding solvent and that excitation to the Franck–Condon state does not cause a significant change in dipole moment; the computed dipole moment^[28] is 8.8 D for the solute in CHCl_3 .

Fluorescence is apparent with an emission maximum (λ_{FLU}) at 510 nm in MTHF (Figure 4b). The spectral profile is similar to that of the lowest-energy absorption transition, with a broad, featureless band that resembles what might reasonably be expected for an intramolecular charge-transfer transition.^[34] Fitting the reduced emission spectrum^[32] to a small series of Gaussian components (Figure 4b), each with a FWHM of 2135 cm^{-1} , indicates that the 0,0 transition for relaxed fluorescence lies at $20\,770\text{ cm}^{-1}$ (i.e., 480 nm). This translates to an effective Stokes shift of 4255 cm^{-1} while the corresponding Huang–Rhys factor (S_{M})^[35] for the relaxed emission transition is

0.83. The latter was calculated^[36] from Equation (1) where I refers to relative intensity as measured by the area of the respective Gaussian component. The term M refers to an averaged medium-frequency vibration associated with vibronic modes $m = 1, 2, 3$, etc. For conjugated polymers,^[37] S_{M} is directly proportional to the effective conjugation length but for small molecules is usually taken as an indication of the exciton-phonon coupling strength.^[38]

$$I_{0,m} = \frac{e^{-S_{\text{M}}} S_{\text{M}}^m}{m!} \quad (1)$$

Similar emission spectra are observed in toluene ($\lambda_{\text{FLU}} = 505\text{ nm}$) and cyclohexane ($\lambda_{\text{FLU}} = 470\text{ nm}$) at room temperature and the parameters extracted from a Gaussian analysis are collected in Table S6. In each solvent, the excitation spectrum remains in good agreement with the absorption spectrum for the lowest-energy transition (Figure 4c) while there is reasonably close comparability of the parameters extracted from the Gaussian analyses (Table S6). The FWHM for the fluorescence profile remains relatively large, corresponding to a mean value of $1910 \pm 300\text{ cm}^{-1}$, indicating that the total re-organisation energy associated with the transition from the relaxed excited-singlet state is substantial; the approximate value for E_{N} derived from the Gaussian fitting is 1935 cm^{-1} (i.e., 0.24 eV) in MTHF. The mean vibronic mode ($h\omega_{\text{M}}$) that accompanies deactivation of the relaxed excited-singlet state has a value of 1390 cm^{-1} , corresponding to aromatic stretching vibrations associated with the heterobicyclic ring structure.

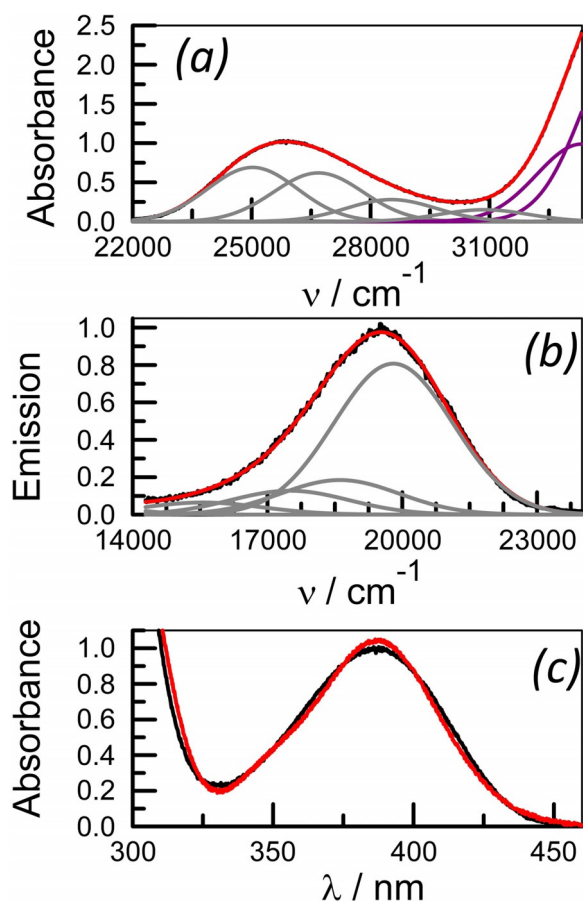


Figure 4. Optical spectra recorded for LB(O) in MTHF at room temperature. Indicating deconstruction of (a) reduced absorption and (b) reduced fluorescence spectra into Gaussian components. The experimental (black curve) and reconstructed (red curve) spectra are compared while the individual Gaussian components are given as grey curves. (c) Comparison of absorption (black curve) and excitation (red curve) spectra. N.B. The indigo curves on panel (a) refer to absorption to a higher-lying state.

Fluorescence from LB(O) in fluid solution at ambient temperature is weak; the fluorescence quantum yield (Φ_F) being 0.012 ± 0.001 in toluene. Furthermore, time-resolved emission profiles were not properly represented^[39] by a single exponential component. More than 98% of the signal decayed with a lifetime of 0.74 ± 0.05 ns but a good statistical fit^[40] required the inclusion of a longer-lived component. This latter lifetime was difficult to resolve with real accuracy but is in the range 2.8 ± 0.5 ns. It is possible that this second component belongs to an impurity but, if so, its spectral profile remains comparable to that of the dominant emitting species. The radiative rate constant (k_{RAD}) for the relaxed excited state in toluene is $1.6 \times 10^7 \text{ s}^{-1}$. The photophysical properties recorded in MTHF are collected in Table 2 for convenience.

Slow cooling of the solution to 77 K, where MTHF forms a rigid glass,^[41] causes a modest red shift for the entire emission envelope (Figure 5). Now, the 0,0 transition is located at 19615 cm^{-1} , which corresponds to a red shift of $1,115 \text{ cm}^{-1}$ compared to fluid solution. It is notable that in the rigid glass there is a small amount of what might be termed “hot” emis-

Table 2. Compilation of the photophysical properties recorded for the two <i>tert</i> -leucine complexes in MTHF.		
Parameter	LB(O)	LB(N)
λ_{ABS} [nm]	390	490
ϵ_{MAX} [$\text{M}^{-1} \text{cm}^{-1}$]	12 900	17 400
$f^{\text{[a]}}$	0.22	0.24
λ_{FLU} [nm]	510	610
$SS^{\text{[b]}}$ [cm^{-1}]	4255	2830
Φ_F	0.009	0.017
τ_S [ns]	0.33	0.42
k_{RAD} [10^7 s^{-1}]	2.7	4.0
$\tilde{\nu}_{0,0}$ [cm^{-1}] ^[c]	20 770	16 915

[a] Oscillator strength calculated for the lowest-energy, intramolecular charge-transfer transition. [b] Stokes shift calculated on the basis of the Gaussian band-shape analysis. [c] Wavenumber for the 0,0 transition identified by the Gaussian analysis.

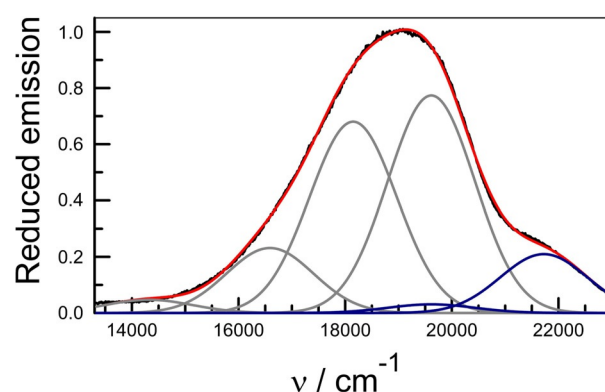


Figure 5. Experimental (black curve) and simulated (red curve) emission spectra recorded for LB(O) in MTHF at 77 K. Components related to the higher-energy Franck-Condon state are shown in blue while the vibronic bands associated with the relaxed geometry are indicated as grey curves.

sion on the high-energy side of the fluorescence profile (Figure 5). The 0,0 band for this new emission, which is seen only in the rigid glass at temperatures below 105 K, occurs at $21\,725 \text{ cm}^{-1}$, which places the emitting state at ca. 2100 cm^{-1} above the relaxed excited-singlet state. We attribute this higher-energy emission to the Franck-Condon state^[42] formed by direct excitation.

Optical properties of LB(N)

The photophysical properties for LB(O) are not promising in terms of developing new fluorogenic sensors^[1,15,16] and it appears that there is a competing radiationless channel that quickly depletes the excited-state population. This behaviour is in marked contrast to that seen for BODIPY^[2,3] and BOPHY^[7,8] derivatives but is reminiscent of the situation found with the BORANILS^[9,43] and other B(III) chelates.^[1] In an attempt to improve the optical properties, including a shift to longer wavelength,^[6] the oxygen atom in the heterobicyclic ring was replaced with an *N*-CH₃ group. This simple substitution has the effect of causing a red shift of ca. 100 nm. Now, λ_{ABS} appears at ca. 490 nm in MTHF with ϵ_{MAX} increasing to $17,400 \text{ M}^{-1} \text{ cm}^{-1}$; a

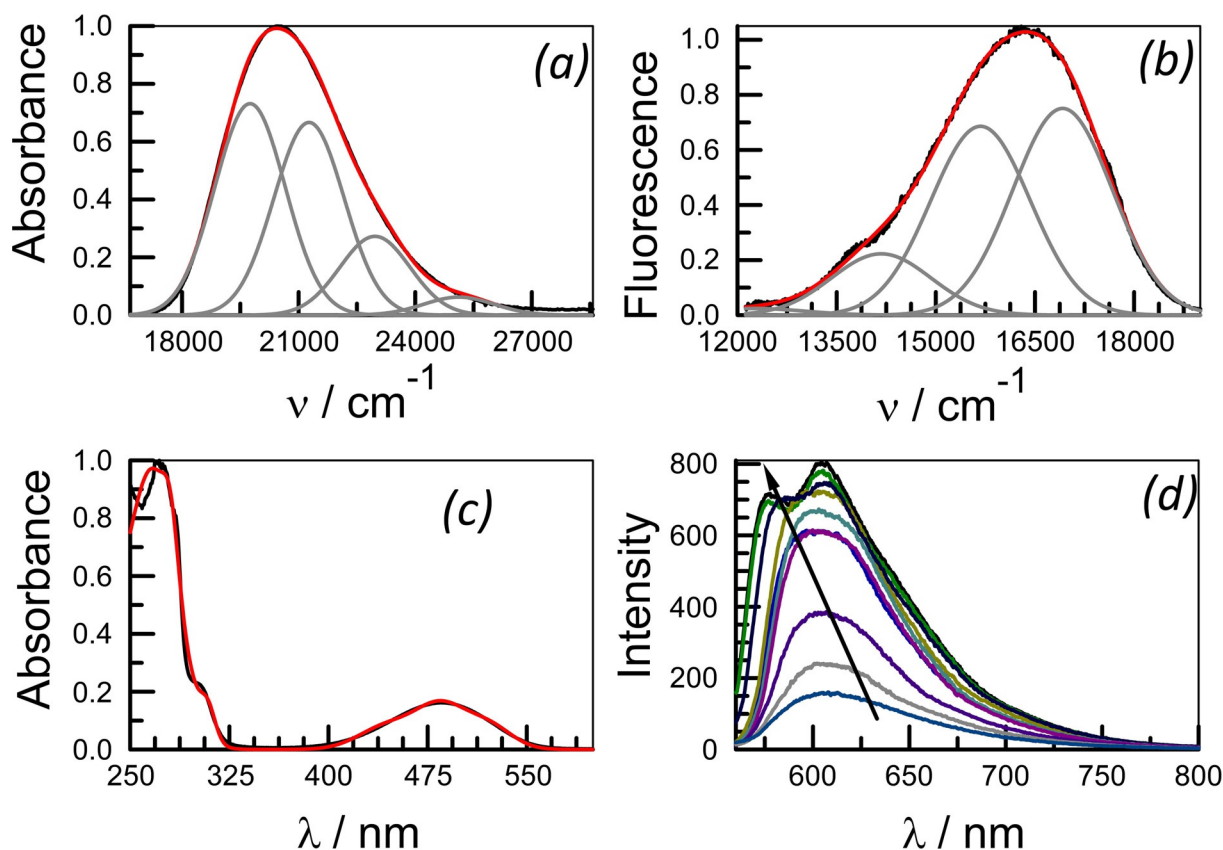


Figure 6. (a) First-allowed absorption transition, shown as a reduced spectrum, recorded for LB(N) in MTHF and the corresponding deconstruction into Gaussian components. (b) Corresponding reduced fluorescence spectrum and assigned Gaussian components recorded in MTHF with excitation at 485 nm. (c) Comparison of absorption (black curve) and excitation (red curve) spectra recorded for LB(N) in MTHF and showing the higher-energy transitions. (d) Effect of lowering the temperature on the fluorescence spectrum recorded for LB(N) in MTHF. The arrow indicates the course of decreasing temperature.

similar red shift occurs for the so-called aza-BODIPY dyes.^[6] The lower energy region of the spectrum is relatively simple and can be deconstructed into a progression of Gaussian components^[32] (Figure 6a). This locates the 0,0 transition at 19750 cm^{-1} . The vibronic mode associated with Franck-Condon excitation has an average value of ca. 1520 cm^{-1} and there is only a modest effect of solvent on the spectral fitting parameters (Table S7). More intense transitions are located in the region below 300 nm (Figure 6).

Weak fluorescence is observed for LB(N) in MTHF at room temperature with a maximum centred at ca. 16500 cm^{-1} (i.e., 610 nm) as shown in Figure 6b. Similar emission spectra are seen in cyclohexane and toluene (Table S7). The excitation spectrum matches well with the absorption envelope over the entire wavelength range (Figure 6c). Gaussian profile analysis for the reduced emission spectrum shows that the entire fluorescence spectrum can be deconstructed into a small series of vibrational bands with common FWHM of 1775 cm^{-1} . The 0,0 transition lies at 16915 cm^{-1} which corresponds to an effective Stokes shift of 2830 cm^{-1} in MTHF. The Huang–Rhys factor^[35] of 0.91 is comparable to that found for LB(O), and identical to that determined for the corresponding absorption transition, while the accompanying vibronic mode is 1240 cm^{-1} . Similar parameters are recovered for fluorescence spectra recorded in toluene and cyclohexane and the results are summarised in

Table S6. It can be seen that the nature of the solvent has little effect on the energy of the 0,0 transition, the FWHM or the S_M although only a few solvents have been studied. In each case, however, the Stokes shift remains markedly smaller than that found for LB(O).

It is clear that replacing the heterobicyclic O atom with an $N\text{-CH}_3$ group has a profound effect on the optical properties of the chromophore. In particular, the Stokes shift is decreased significantly. Unfortunately, this replacement does not enhance fluorescence and at room temperature Φ_F is only 0.048 ± 0.005 in toluene solution. Similar values are found in cyclohexane. Time-resolved fluorescence studies give rise to a τ_5 value of $0.60 \pm 0.08\text{ ns}$ in toluene. As such, the radiative rate constant has an approximate value of $8 \times 10^7\text{ s}^{-1}$ at room temperature. Fluorescence is weaker in MTHF at room temperature (Table 2), where k_{RAD} falls to $4 \times 10^7\text{ s}^{-1}$.

On lowering the temperature of the MTHF solution, the fluorescence yield increases slightly over the range where the solvent remains liquid^[44] (Figure 6d); it might be recalled that MTHF freezes at 137 K to form an amorphous phase but does not develop into a rigid glass until around 100 K.^[41] This increased emission yield, which is accompanied by a small blue shift, follows Arrhenius behaviour but the corresponding activation energy ($E_A = 130\text{ J mol}^{-1}$) is unusually small (Figure S28). Deactivation of the relaxed singlet-excited state, therefore, is

essentially activationless in fluid MTHF. As the solvent begins to rigidify, a new fluorescence band appears at higher energy (Figure 6d). This latter species can be assigned to the initial Franck–Condon state.^[42]

The fluorescence quantum yield remains well below unity in the low temperature region. This indicates that, even in a rigid environment, there is a process that competes effectively with radiative decay. A possible activationless channel for deactivation of the excited-singlet state involves intersystem crossing to the triplet manifold, although this is not a common occurrence for boron(III) chelates.^[45] To confirm triplet formation, a series of laser flash photolysis studies was made with excitation (FWHM = 4 ns) at 532 nm. In deoxygenated toluene solution, a transient absorption signal was detected with a maximum at 350 nm (Figure S29). This species decays via first-order kinetics to restore the pre-pulse baseline with a mean lifetime of $95 \pm 10 \mu\text{s}$ (Figure S30). Comparable properties were recorded in CHCl_3 and acetonitrile solution. In each case, the lifetime was shortened in the presence of molecular oxygen and, on this basis, the transient is attributed to the triplet-excited state. It was not possible to obtain a meaningful phosphorescence signal in MTHF at 77 K.

A thin film was prepared by casting a concentrated solution of LB(N) in CHCl_3 onto a quartz microscope slide and drying at room temperature (Figure S32). The absorption spectrum remained remarkably similar to that recorded in fluid solution, with the lowest-energy absorption band being centred at 488 nm (Figure 7). Furthermore, the spectral profile is identical to that observed in solution. Under excitation at 480 nm, the film displays orange fluorescence with an emission maximum at 600 nm (Figure 7). Again, the emission spectrum closely resembles that recorded in solution while the excitation spectrum matches quite well with the absorption spectrum (Figure 7). The averaged fluorescence quantum yield, measured with the aid of an integrating sphere,^[46] was found to be 0.19 ± 0.04 while time-resolved fluorescence spectroscopy showed the decay kinetics were non-exponential. A satisfactory fit could be obtained using a dual-exponential fit with lifetimes of 0.45 ns (15%) and 2.25 ns (85%). That the bulk of the emission decays with a relatively long lifetime is further testament to the capacity of the solid environment^[47] to inhibit the fast

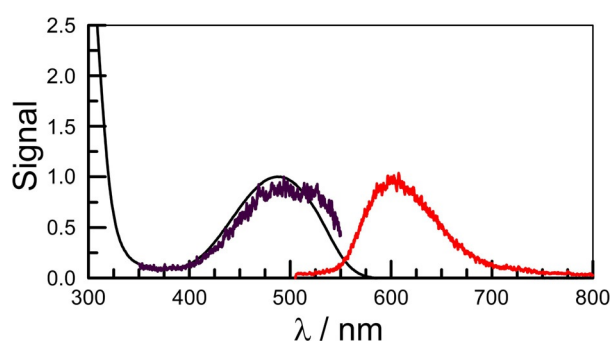


Figure 7. Absorption (black curve), fluorescence (red curve) and excitation (indigo curve) spectra recorded for a thin film of LB(N) cast from CHCl_3 solution. Each measurement was the average of five separate spectra.

radiationless deactivation process that has such a deleterious effect in solution.

The optical properties recorded for the thin film are similar to those measured for LB(N) in cyclohexane solution at ambient temperature. There is no indication for hot emission and fluorescence appears solely from the relaxed excited state. It is important to note that the Stokes shift remains significant in the thin film such that self-absorption,^[48] which is a serious problem for many solid-state materials,^[49] is unimportant. The increased quantum yield and lifetime can be used to argue that the competing radiationless decay channel is essentially closed down in the thin film. If so, this could be the direction to take in terms of finding useful functions for these reagents. It is important, however, to first confirm the anticipated chirality.

Circular dichroism

The inherent chirality of the new chromophores was investigated by electronic circular dichroism (ECD) spectroscopy. The ECD spectra recorded in CHCl_3 as solvent are depicted in Figure 8. The enantiomerically pure samples of both compounds, obtained solely from selection of the starting *tert*-leucine residue, display perfect mirror image ECD patterns (Figure S31). To assign the absolute stereochemistry, the calculated spectra were compared with spectral predictions based on quantum chemical TD-DFT calculations. The calculations were performed using both B3LYP and CAM-B3LYP functionals and the 6–311-G(3df,2pd) basis set. The CAM-B3LYP functional is generally considered to be an excellent functional for such calculations,^[13,50] but this is not universal and, in cases where there is pronounced intramolecular charge-transfer character, other functionals perform better.^[51] In our work, we repeated the calculations making use of the standard B3LYP functional.^[52]

By comparison to the experimental absorption spectra, the computational studies overestimate the excitation energies, especially for the CAM-B3LYP functional. This situation is far from unusual.^[53] However, the spectral patterns for both *syn/anti*-LB(O) and *syn/anti*-LB(N) are more accurately represented by the CAM-B3LYP calculations. For LB(O), the experimental local minimum between the two main absorption transitions, located at around 300 nm, is not predicted by the B3LYP functional. Moreover, the negative contribution in the $-/+$ couplet centred in the ECD spectrum at 300 nm is not as pronounced as is the case for the CAM-B3LYP spectrum. Similar disparity can be found in the spectra of LB(N) at the B3LYP level: the UV/Vis absorption does not reach the baseline between the two major bands and a prominent positive ECD band is wrongly predicted at 350 nm. Based on the CAM-B3LYP calculations, the stereochemistry around the boron site for both compounds can be confirmed. The experimental spectra illustrated in Figure 8 therefore are identified as the *D*-configured species.

The optical absorption properties appear to be less affected by the stereochemistry of the second chiral centre. The absorption spectra of the *syn*- and *anti*-forms are closely comparable, although in the case of LB(O) there is a small, but significant,

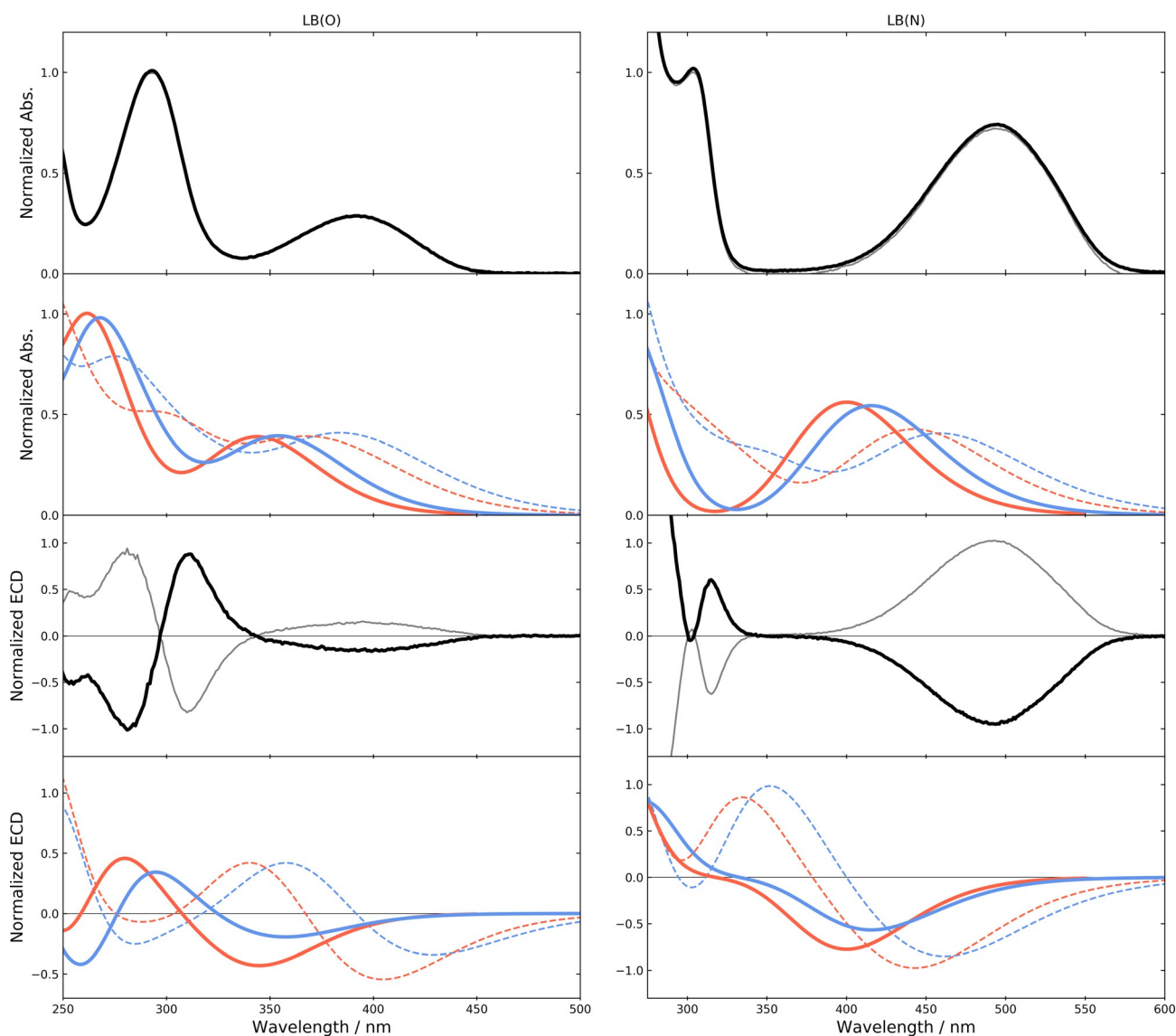


Figure 8. Experimental optical absorption and ECD spectra recorded for LB(O) (left) and LB(N) (right) for the *D*-*syn* (black) and *L*-*syn* (grey) configurations. The calculated UV-vis and ECD spectra of the *D*-*syn* (blue) and *D*-*anti* (orange) configurations, computed at the CAM-B3LYP/6-311++G(3df,2pd) (full line) and B3LYP/6-311++G(3df,2pd) (dashed line) levels of theory.

difference at lower wavelengths. However, the magnitudes of the $-/+$ ECD couplet bands observed around 275 nm for the *syn*-configuration better mimic the experimental data. Thus, for LB(O), there is a definite preference for the *syn*-form, thereby confirming its full stereochemistry, whereas for LB(N) any assignment regarding the carbon asymmetric centre remains inconclusive. Interestingly, the leucine residue does not play a significant role in establishing the optical absorption properties, which are dominated by intramolecular charge-transfer interactions.

Because of their invaluable optical and opto-electronic properties, there have been numerous prior reports of chiral B(III) chelates. For example, a new class of chiral BODIPYs was introduced^[54] recently whereby chiral carbon atoms are attached directly to the boron centre. These compounds, by taking advantage of the inherent absorption and fluorescence properties of the BODIPY nucleus, look promising in terms of ad-

vanced chiroptical properties, including circularly polarised luminescence. A more common method^[55] for preparation of chiral BODIPYs is to introduce a chiral perturber in the vicinity of the boron atom^[13] and resolve the mixture of diastereoisomers. Chiral BOPHY derivatives have been reported^[56] wherein the fluorine atoms are replaced by enantiopure binaphthols, endowing the chromophore with chiroptical activity. This strategy, however, leads to a marked decrease in fluorescence because of the introduction of an intramolecular charge-transfer state. Chiral BORANILs have been synthesized from chiral benzylamines.^[57] These latter BF_2 -complexes exhibit blue fluorescence in solution and in the solid state but the source of chirality is remote from the boron centre and this affects the circular dichroism of the complexes. The new *tert*-leucine complexes compare favourably, in terms of providing easy access to chiral chromophores, with any literature example.

Conclusions

This investigation reports on a simple synthetic strategy that introduces chirality into the molecular backbone of a rigid boron(III) chelate. Both *N,N,O* and *N,O,O* bonding motifs have been realized and a key feature of the synthetic procedure is that the resultant diastereoisomers are resolved prior to condensation. Mild reaction conditions are used for coupling of the starting materials, without the need for a large excess of one reagent, and it is anticipated that the one-pot protocol could be adapted to generate a wide range of functionalized derivatives. The final compounds have reasonably high dipole moments and are soluble in most organic solvents, but not water. They can be crystallized readily from solution, retaining the imported chirality, to give interesting 3-dimensional structures. The *N,O,O* species, in particular, has high thermal and photochemical stability. As a new family of chromophores, these *tert*-leucine complexes are only weakly fluorescent in solution, even in non-polar solvents. The *N,N,O* derivative is significantly more fluorescent when prepared in the form of a thin film, cast from CHCl_3 solution. This is a further example of what has become known as aggregation-induced emission.^[58]

It has to be mentioned that a somewhat related *N,O,O* boron-fused azomethine complex having a stereogenic boron centre was reported recently.^[13] In this case, chiral resolution of the racemic mixture was achieved by high-performance liquid chromatography using an amylose-based stationary phase. As found for the *tert*-leucine complexes, these compounds are only weakly fluorescent in solution but are more strongly emissive in the crystalline phase.^[13] There is, therefore, a high degree of similarity with LB(O), although no analogue of LB(N) exists. The main difference between LB(O) and the boron-fused azomethine complex relates to the ease of obtaining resolved enantiomers.

In common with the BORANIL family of boron(III) chelates^[9,43] and these new *N,O,O* boron-fused azomethine complex,^[13] the *tert*-leucine derivatives have little propensity for the development of fluorescent labels or sensors, at least in solution. The problem relates to a radiationless channel that rapidly deactivates the excited-singlet state. This channel involves intramolecular charge-transfer processes^[43] which, in the first instance, promote translation of the Franck–Condon state to a relaxed excited-singlet state. This internal relaxation is hindered in the thin film, thereby stabilising the Franck–Condon state and favouring fluorescence. Unlike the situation reported for the BORANILS,^[9] fluorescence is only partially recovered in non-polar solvents for the *tert*-leucine complexes. The same is true at low temperature where fluorescence from the Franck–Condon state has to compete with an important radiationless channel.

Experimental Section

Synthesis and characterisation

(3*R*,11*R*)-3-(*tert*-butyl)-11-phenyl-11*H*-4*I*4,11*I*4-benzo[e][1,3,2]oxazaborolo[2,3-*b*][1,3,2]oxazaborinin-2(3*H*)-one *D*-*syn*-LB(O). A

suspension of *D*-*tert*-leucine (0.200 g, 1.52 mmol, 2.0 equiv) and salicylaldehyde (0.139 g, 1.14 mmol, 1.5 equiv) in distilled water (2.0 mL) was stirred at 90 °C for 1 h after which phenylboronic acid (0.092 g, 0.762 mmol, 1 equiv) was added and the mixture was then stirred at 90 °C for 20 h. The reaction mixture, which appeared as a biphasic composition of a precipitate and a supernatant liquid, was filtered and the solid retained in the filter was then washed with water followed by hexane. The desired compound was recovered from the filter with dichloromethane, which was subsequently removed under reduced pressure to afford *D*-*syn*-LB(O) (0.237 g, 97%) as a greenish solid, m.p. 274–281 °C. ¹H NMR (500 MHz, CDCl_3) δ 8.34 (s, 1H), 7.57–7.48 (m, 2H), 7.39–7.35 (m, 2H), 7.24–7.17 (m, 3H), 7.03–6.97 (m, 2H), 4.04 (d, J = 1.0 Hz, 1H), 1.02 ppm (s, 9H). ¹¹B NMR (128 MHz, CDCl_3) δ 6.80 ppm. ¹³C NMR (126 MHz, CDCl_3) δ 169.92, 162.89, 160.08, 139.19, 131.24, 130.29, 127.90, 127.57, 120.70, 120.35, 119.03, 74.70, 35.60, 27.21 ppm. IR (neat): $\tilde{\nu}_{\text{max}}$ = 2968, 1733, 1633, 1556, 1453, 1293, 1197, 1133, 992, 980, 766, 702, 455 cm^{-1} . HRMS (ESI): m/z found: $[M+H]^+$ 322.1615, $\text{C}_{19}\text{H}_{20}\text{BNO}_3$ requires $[M+H]^+$ 322.1618.

(3*R*,11*R*)-3-(*tert*-butyl)-10-methyl-11-phenyl-10,11-dihydro-4*I*4,11*I*4-benzo[d][1,3,2]oxazaborolo[3,2-*a*][1,3,2]diazaborinin-2(3*H*)-one *D*-*syn*-LB(N). A mixture of *D*-*tert*-leucine (0.097 g, 0.739 mmol, 1.0 equiv), 2-(methylamino)benzaldehyde (0.100 g, 0.739 mmol, 1 equiv) and phenylboronic acid (0.090 g, 0.739 mmol, 1 equiv) in toluene (10 mL) was stirred at 90 °C for 24 h during which the colour changed from yellow to dark red. The resulting solid product was filtered, washing three times with water and petroleum ether. Purification by flash column chromatography on silica, eluting with ethyl acetate/petroleum ether 1:1 gave the boron chelate *D*-*syn*-LB(N) (0.185 g, 74%) as a red solid, m.p. 197–201 °C. ¹H NMR (300 MHz, CDCl_3) δ 7.94 (s, 1H), 7.33–7.23 (m, 3H), 7.19 (dd, J = 8.0, 1.6 Hz, 1H), 7.13–7.07 (m, 3H), 6.56 (d, J = 8.9 Hz, 1H), 6.50 (ddd, J = 7.9, 6.9, 0.9 Hz, 1H), 3.84 (d, J = 0.8 Hz, 1H), 2.71 (s, 3H), 0.88 ppm (s, 9H). ¹³C NMR (75 MHz, CDCl_3) δ 171.68, 160.12, 151.15, 138.32, 132.93, 129.89, 127.38, 127.33, 115.09, 115.00, 113.47, 75.11, 35.25, 31.20, 27.43 ppm. ¹¹B NMR (96 MHz, CDCl_3) δ 5.27 ppm. IR (neat): $\tilde{\nu}_{\text{max}}$ = 2958, 1742, 1625, 1472, 1365, 1255, 978, 747, 702, 607 cm^{-1} . HRMS (ESI): m/z found: $[M+H]^+$ 335.1932, $\text{C}_{20}\text{H}_{23}\text{BN}_2\text{O}_2$ requires $[M+H]^+$ 335.1935.

Crystallography

Single crystal diffraction data were collected at 150 K on an Xcalibur, Atlas, Gemini ultra-diffractometer equipped with an Oxford Cryosystems CryostreamPlus open-flow N_2 cooling device using copper radiation ($\lambda_{\text{CuK}\alpha}$ = 1.54184 Å). The intensities were corrected for absorption using a multifaceted crystal model created by indexing the faces of the crystal for which data were collected.^[59] Cell refinement, data collection and data reduction were undertaken via the software CrysAlisPro.^[60] All structures were solved using XT^[61] and refined by XL^[62] using the Olex2 interface.^[63] All non-hydrogen atoms were refined anisotropically and hydrogen atoms were positioned with idealised geometry. The displacement parameters of the hydrogen atoms were constrained using a riding model with U(H) set to be an appropriate multiple of the Ueq value of the parent atom.

Deposition numbers 2048356 (for LB(O)), and 2048355 (for LB(N)) contain the supplementary crystallographic data for this paper. These data are provided free of charge by the joint Cambridge Crystallographic Data Centre and Fachinformationszentrum Karlsruhe Access Structures service.

Circular dichroism

All four samples were dissolved in CHCl_3 as follows: L-*syn*-LB(O) ca. 0.5 mg in 150 μL ; D-*syn*-LB(O) ca. 0.5 mg in 150 μL ; L-*syn*-LB(N) ca. 0.5 mg in 300 μL ; D-*syn*-LB(N) ca. 0.5 mg in 200 μL . Measurements were performed with a SUPRASIL® quartz cell (Hellma BeNeLux, Krübeke, BE) having a path length of 0.05 cm. Prior to making a sample measurement, a solvent background scan was recorded using a Chirascan™-Plus spectrophotometer (Applied Photophysics Ltd, Leatherhead, UK). The instrument was flushed continuously with nitrogen gas (4 L min^{-1} flow rate) and the temperature of the sample chamber was kept at 20 °C. The spectral range was 180–800 nm, with a bandwidth of 1 nm and at an acquisition time of 0.1 s nm^{-1} . The spectral text files were generated after subtraction of the solvent background. All ECD calculations were performed using the Gaussian 16, revision A.03 program^[64] and using preliminary structural data obtained from Molecular Mechanics based GMMX conformational search routines with Gaussview-6.^[65] The spectral simulations were performed by the TD-DFT method, considering 100 singlet-excited states. Both B3LYP/6-311-G(3df,2pd) and CAM-B3LYP/311-G(3df,2pd) levels were used in all cases. The computed spectra were artificially line-broadened using a Gaussian band shape ($\sigma=0.3$ eV). Corrections for solvent influences were made using the integral equation formalism model (IEFPCM; as implemented in Gaussian 16) and a dielectric constant for chloroform of 4.7113.

Electrochemistry

Cyclic voltammetry was made with a conventional 3-electrode system using a highly polished, glassy carbon working electrode. The counter electrode was a Pt wire and the reference electrode was an Ag/Ag⁺ electrode maintained in acetonitrile. The background electrolyte was ammonium tetra-*N*-butylammonium perchlorate (0.2 M) and the solvent was freshly distilled CH_2Cl_2 . An E600 potentiostat (CH Instruments) was used with a scan rate of 60 mV s^{-1} . Solutions were purged with N_2 before the experiment and maintained in an O_2 -free environment throughout the scan.

Spectroscopic studies

Spectroscopic-grade solvents were purchased from commercial sources and used as received after ensuring the absence of fluorescent impurities. For all solution-phase studies, absorption spectra were recorded with a Hitachi U-3310 spectrophotometer while steady-state fluorescence studies were made with an Yvon-Jobin Fluorolog tau-3 spectrometer. Spectra were recorded at ambient temperature unless stated otherwise. All fluorescence spectra were recorded under optically dilute conditions and were supported by excitation spectra. Experimental data were extracted from the instrument and processed separately to provide reduced spectra for Gaussian band-shape analyses.^[6a] Fluorescence quantum yields were determined by reference to known standards used at optically dilute concentrations. Fluorescence quantum yields were measured relative to phenanthrene^[66] in ethanol ($\Phi_F=0.125$) and zinc(II) meso-tetraphenylporphyrin in toluene.^[67] Corrections were made for changes in refractive index.^[68] Fluorescence lifetimes were recorded by time-correlated, single photon counting methods with high intensity, short duration laser diodes as excitation source. These diodes provided discrete excitation wavelengths of 375 nm (FWHM = 130 ps) and 515 nm (FWHM = 140 ps). Fluorescence was isolated from scattered excitation light using a high-radiance monochromator and detection was made with a micro-channel plate PMT operated at -20 °C. Data analysis^[39] was made

by standard statistical methods. Temperature dependence studies were made with an Oxford Instruments Optistat DN using dilute solutions of the fluorophore in freshly distilled MTHF solution.

Time-resolved transient absorption measurements were obtained with an Applied Photophysics LKS-70 system using a 4-ns pulsed Quantel Brilliant B Nd:YAG laser with the 1064 nm output being frequency doubled to 532 nm. The repetition rate of the laser was 10 Hz with the power varying from 1–45 mJ per pulse. Appropriate excitation wavelengths were selected with an OPO pumped by the second or third harmonic of the Q-switched Nd:YAG laser. As necessary, samples were saturated with nitrogen for 20 min before starting the experiment. For kinetic measurements made at a fixed wavelength, 200 individual laser shots were averaged for each sample and solvent under the same experimental conditions, and three different laser intensities were used. Metal screen filters were employed to obtain the different laser intensities. The signals were detected with a PMT having a 5 stage dynode chain for high current linearity, amplified by a preamplifier, recorded by a digital oscilloscope (Tektronix DPO7254C), and subsequently transferred to a PC for data analysis and storage. A plane ruled grating, 1800 g mm^{-1} , with 500 nm blaze, was used as standard. The average spectral dispersion was 1.8 nm mm^{-1} . On a single shot basis, the sensitivity of the absorption change at 500 nm was ca. 0.0005. Analysis of the background corrected signals was made using in-house software.

Acknowledgements

We thank Newcastle University for financial support of this work. H.H.T.A.-S. acknowledges the award of a research scholarship from The Umm Al-Qura University (Saudi Arabia). N.A. thanks the Saudi Arabian Cultural Bureau for financial support in the form of a King Abdullah Scholarship. The University of Antwerp (BOF-NOI) is acknowledged for the pre-doctoral scholarship of R.A. The resources and services used in this work were provided by the VSC (Flemish Supercomputer Center), funded by the Research Foundation—Flanders (FWO) and the Flemish Government.

Conflict of interest

The authors declare no conflict of interest.

Keywords: boron(III) chelates · charge-transfer interactions · chromophores · circular dichroism · photophysics

- [1] H. H. T. Al-Sharif, A. Harriman in *Bio-Inspired Artificial Light-Harvesting Arrays Based on Boron(III)-Chelates, Recent Advances in Boron-Containing Materials* (Ed.: M. Aydin), IntechOpen, 2020.
- [2] a) A. Loudet, K. Burgess, *Chem. Rev.* **2007**, *107*, 4891–4932; b) G. Ulrich, R. Ziessel, A. Harriman, *Angew. Chem. Int. Ed.* **2008**, *47*, 1184–1201; *Angew. Chem.* **2008**, *120*, 1202–1219.
- [3] a) N. Boens, V. Leen, W. Dehaen, *Chem. Soc. Rev.* **2012**, *41*, 1130–1172; b) A. Kamkaew, S.-H. Lim, H.-B. Lee, L. V. Kiew, L.-Y. Chung, K. Burgess, *Chem. Soc. Rev.* **2013**, *42*, 77–88; c) R. Ziessel, G. Ulrich, A. Harriman, *New J. Chem.* **2007**, *31*, 496–501; d) T. Kowada, H. Maeda, K. Kikuchi, *Chem. Soc. Rev.* **2015**, *44*, 4953–4972; e) S.-G. Awuah, Y. You, *RSC Adv.* **2012**, *2*, 11169–11183.
- [4] a) J. P. Lewtak, D. T. Gryko, *Chem. Commun.* **2012**, *48*, 10069–10086; b) M. A. Filatov, A. Y. Lebedev, S. N. Mukhin, S. A. Vinogradov, A. V. Cheprakov, *J. Am. Chem. Soc.* **2010**, *132*, 9552–9554; c) Y. Kubo, Y. Minowa,

- T. Shoda, K. Takeshita, *Tetrahedron Lett.* **2010**, *51*, 1600–1602; d) T. Sarma, P. K. Panda, J.-I. Setsune, *Chem. Commun.* **2013**, *49*, 9806–9808; e) H. Ito, H. Sakai, Y. Suzuki, J. Kawamata, T. Hasobe, *Chem. Eur. J.* **2020**, *26*, 316–325.
- [5] a) R. Ziessel, A. Harriman, *Chem. Commun.* **2011**, *47*, 611–631; b) F. Bergström, I. Mikhalyov, P. Hagglof, R. Wortmann, T. Ny, L. B. A. Johansson, *J. Am. Chem. Soc.* **2002**, *124*, 196–204; c) M. Bröring, R. Kruger, S. Link, C. Kleeberg, S. Kohler, X. Xie, B. Ventura, L. Flamigni, *Chem. Eur. J.* **2008**, *14*, 2976–2983; d) Y. Hayashi, S. Yamaguchi, W.-Y. Cha, D. Kim, H. Shinokubo, *Org. Lett.* **2011**, *13*, 2992–2995; e) J. Iehl, J.-F. Nierengarten, A. Harriman, T. Bura, R. Ziessel, *J. Am. Chem. Soc.* **2012**, *134*, 988–998.
- [6] J. K. G. Karlsson, A. Harriman, *J. Phys. Chem. A* **2016**, *120*, 2537–2546.
- [7] I. S. Tamgho, A. Hasheminasab, J. T. Engle, V. N. Nemykin, C. J. Ziegler, *J. Am. Chem. Soc.* **2014**, *136*, 5623–5626.
- [8] a) O. J. Woodford, R. Ziessel, A. Harriman, C. Wills, A. A. Alsimaree, J. G. Knight, *Spectrochim. Acta Part A—Mol. Biomol. Spectrosc.* **2019**, *208*, 57–64; b) O. J. Woodford, P. Stachelek, R. Ziessel, N. Algoazy, J. G. Knight, A. Harriman, *New J. Chem.* **2018**, *42*, 4835–4842; c) Y. V. Zatsikha, D. B. Nemez, R. L. Davis, S. Singh, D. E. Herbert, A. J. King, C. J. Ziegler, V. N. Nemykin, *Chem. Eur. J.* **2017**, *23*, 14786–14796; d) S. Boodts, E. Fron, J. Hofkens, W. Dehaen, *Coord. Chem. Rev.* **2018**, *371*, 1–10.
- [9] D. Frath, S. Azizi, G. Ulrich, P. Retailleau, R. Ziessel, *Org. Lett.* **2011**, *13*, 3414–3417.
- [10] a) O. J. Woodford, R. Ziessel, A. Harriman, *ChemPhotoChem* **2018**, *2*, 1046–1054; b) O. J. Woodford, A. Harriman, W. McFarlane, C. Wills, *ChemPhotoChem* **2017**, *1*, 317–325.
- [11] H. H. T. Al-Sharif, R. Ziessel, P. G. Waddell, C. Dixon, A. Harriman, *J. Phys. Chem. A* **2020**, *124*, 2160–2172.
- [12] a) D. Frath, A. Poirel, G. Ulrich, A. De Nicola, R. Ziessel, *Chem. Commun.* **2013**, *49*, 4908–4910; b) I. Kaur, S. Shivani, P. Kaur, K. Singh, *Dyes Pigm.* **2020**, *176*, 108198; c) G.-J. Yin, X.-J. Chu, T. Zhang, H.-F. Mao, C.-Y. Wang, Y.-F. Yang, *Chin. J. Struct. Chem.* **2018**, *37*, 1994–2002; d) Y. Hattori, T. Ogaki, M. Ishimura, Y. Ohta, M. Kirihata, *Sensors* **2017**, *17*, 2436; e) K. Benelhadj, J. Massue, G. Ulrich, *New J. Chem.* **2016**, *40*, 5877–5884; f) L. Sun, F. Zhang, X.-Y. Wang, F. Qiu, M.-Z. Xue, G. Tregnago, F. Ciacilli, S. Osella, D. Beljonne, X.-L. Feng, *Chem. Asian J.* **2015**, *10*, 709–714; g) E. V. Antina, M. B. Berezin, N. A. Dudina, S. L. Burkova, A. Y. Nikonova, *Russ. J. Inorg. Chem.* **2014**, *59*, 1187–1194; h) L. F. Smith, B. A. Blight, H.-J. Park, S. Wang, *Inorg. Chem.* **2014**, *53*, 8036–8044; i) M. J. Mayoral, M. Cano, J. A. Campo, J. V. Heras, E. Pinilla, M. R. Torres, *Inorg. Chem. Commun.* **2004**, *7*, 974–978.
- [13] S. Ohtani, Y. Takeda, M. Gon, K. Tanaka, Y. Chujo, *Chem. Commun.* **2020**, *56*, 15305–15308.
- [14] R. Clarke, K. L. Ho, A. A. Alsimaree, O. J. Woodford, P. G. Waddell, J. Bogaerts, W. Herrebout, J. G. Knight, R. Pal, T. J. Penfold, M. J. Hall, *ChemPhotoChem* **2017**, *1*, 513–517.
- [15] I. Goradia, J. Doshi, K. Deulker, *Int. J. Curr. Eng. Technol.* **2014**, *4*, 2933–2936.
- [16] a) T. D. James, K. Sandanayake, S. Shinkai, *Nature* **1995**, *374*, 345–347; b) M. T. Reetz, S. Sostmann, *Tetrahedron* **2001**, *57*, 2515–2520; c) X.-M. Chen, N. Hu, H.-W. Wei, H. B. Wang, *J. Fluoresc.* **2020**, *30*, 679–685; d) S. Perrier, C. Ravelet, V. Guieu, J. Fize, B. Roy, C. Perigaud, E. Peyrin, *Biosens. Bioelectron.* **2010**, *25*, 1652–1657; e) G. Beer, K. Rurack, J. Daub, *Chem. Commun.* **2001**, 1138–1139; f) Z.-Y. Jiang, X.-Q. Wang, J.-P. Ma, Z.-P. Liu, *Sci. China Mater.* **2019**, *62*, 355–362; g) N. R. Treich, J. D. Wimpenny, I. A. Kieffer, Z. M. Heiden, *New J. Chem.* **2017**, *41*, 14370–14378; h) Y. Gobo, M. Yamamura, T. Nakamura, T. Nabeshima, *Org. Lett.* **2016**, *18*, 2719–2721; i) S. Kolemen, Y. Cakmak, Z. Kostereli, E. U. Akkaya, *Org. Lett.* **2014**, *16*, 660–663.
- [17] E. Vedejs, R. W. Chapman, S. Lin, M. Müller, D. R. Powell, *J. Am. Chem. Soc.* **2000**, *122*, 3047–3052.
- [18] P. F. Kaiser, J. M. White, C. A. Hutton, *J. Am. Chem. Soc.* **2008**, *130*, 16450–16451.
- [19] a) N. R. Candeias, P. M. S. D. Cal, V. N. André, M. T. Duarte, L. S. F. Veiros, P. M. P. Gois, *Tetrahedron* **2010**, *66*, 2736–2745; b) F. Montalbano, P. M. S. D. Cal, M. A. B. R. Carvalho, L. D. M. Gonçalves, S. D. Lucas, R. C. Guedes, L. S. F. Veiros, R. Moreira, P. M. P. Gois, *Org. Biomol. Chem.* **2013**, *11*, 4465–4472; c) F. Montalbano, J. Leandro, G. D. V. F. Farias, P. R. Lino, R. C. Guedes, J. B. Vicente, P. Leandro, P. M. P. Gois, *RSC Adv.* **2014**, *4*, 61022–61027.
- [20] X. Zhang, J. Yin, J. Yoon, *Chem. Rev.* **2014**, *114*, 4918–4959.
- [21] F. B. M. F. Santos, A. I. Matos, A. E. Ventura, J. O. Gonçalves, L. S. F. Veiros, H. F. Florindo, P. M. P. Gois, *Angew. Chem. Int. Ed.* **2017**, *56*, 9346–9350; *Angew. Chem.* **2017**, *129*, 9474–9478.
- [22] I. A. Apple, O. Meth-Cohn, *Arkivoc* **2002**, *vi*, 4–14.
- [23] a) M. W. Schmidt, K. K. Baldrige, J. A. Boatz, S. T. Elbert, M. S. Gordon, J. H. Jensen, S. Koseki, N. Matsunaga, K. A. Nguyen, S. Su, T. L. Windus, M. Dupuis, J. A. Montgomery, *J. Comput. Chem.* **1993**, *14*, 1347–1363; b) M. S. Gordon, M. W. Schmidt, *Theory and Applications of Computational Chemistry: The First Forty Years* (Eds.: C. E. Dykstra, G. Frenking, K. S. Kim, G. E. Scuseria), Elsevier, Amsterdam **2005**, pp. 1167–1189.
- [24] D. Jacquemin, A. Planchat, C. Adamo, B. Mennucci, *J. Chem. Theory Comput.* **2012**, *8*, 2359–2372.
- [25] C. W. Bauschlicher, H. Partridge, *Chem. Phys. Lett.* **1995**, *240*, 535–540.
- [26] M. Cossi, B. Mennucci, J. Pitarch, J. Tomasi, *J. Comput. Chem.* **1998**, *19*, 833–846.
- [27] C. R. Groom, I. J. Bruno, M. P. Lightfoot, S. C. Ward, *Acta Crystallogr. Sect. B* **2016**, *72*, 171–179.
- [28] A. L. Hickey, C. N. Rowley, *J. Phys. Chem. A* **2014**, *118*, 3678–3687.
- [29] A. J. Bard, L. R. Faulkner, *Electrochemical Methods: Fundamentals and Applications*, 2nd ed., Wiley, New York, **2001**.
- [30] R. Stowasser, R. Hoffmann, *J. Am. Chem. Soc.* **1999**, *121*, 3414–3420.
- [31] a) C.-Y. Jia, S.-X. Liu, C. Tanner, C. Leiggner, A. Neels, L. Sanguinet, E. Levillain, S. Leutwyler, A. Hauser, S. Decurtins, *Chem. Eur. J.* **2007**, *13*, 3804–3812; b) A. D. Laurent, D. Jacquemin, *Int. J. Quantum Chem.* **2013**, *113*, 2019–2039; c) G. Saranya, P. Kolandaivel, K. Senthikumar, *Mol. Phys.* **2013**, *111*, 3036–3046.
- [32] R. Al-Aqar, A. C. Benniston, A. Harriman, T. Perks, *ChemPhotoChem* **2017**, *1*, 198–205.
- [33] A. Gonciarz, R. Pich, K. A. Bogdanowicz, B. Jewloszewicz, W. Przybył, K. Dysz, A. Dylong, A. Kwak, A. Kaim, A. Iwan, J. Rusin, A. Januszko, *Materials* **2019**, *12*, 4191.
- [34] a) M. Maus, W. Rettig, D. Bonafoux, R. Lapouyade, *J. Phys. Chem. A* **1999**, *103*, 3388–3401; b) K. Rechthaler, G. Kohler, *Chem. Phys.* **1994**, *189*, 99–116; c) M. Bixon, J. Jortner, J. Cortes, H. Heitele, M. E. Michel-Beyerle, *J. Phys. Chem.* **1994**, *98*, 7289–7299; d) J. Cortes, H. Heitele, J. Jortner, *J. Phys. Chem.* **1994**, *98*, 2527–2536.
- [35] a) M. Rätsep, J. Linnanto, A. Freiberg, *J. Chem. Phys.* **2009**, *130*, 194501; b) T. Serevičius, P. Adomenas, O. Adomeniene, R. Rimkus, V. Jankauskas, A. Gruodis, K. Kazlauskas, S. Jursenas, *Dyes Pigm.* **2013**, *98*, 304–315.
- [36] M. de Jong, L. Seijo, A. Meijerinka, F. T. Rabouwa, *Phys. Chem. Chem. Phys.* **2015**, *17*, 16959–16969.
- [37] F. A. C. Oliveira, L. A. Cury, A. Righi, R. L. Moreira, P. S. S. Guimarães, F. M. Matinaga, M. A. Pimenta, R. A. Nogueira, *J. Chem. Phys.* **2003**, *119*, 9777.
- [38] W. Barford, M. Marcus, *J. Chem. Phys.* **2014**, *141*, 164101.
- [39] D. V. O'Connor, D. Phillips, *Time-Correlated Single Photon Counting*, Academic Press, London, **1984**.
- [40] M. Van Den Zegel, N. Boens, D. Daems, F. C. De Schryver, *Chem. Phys.* **1986**, *101*, 311–335.
- [41] T. Rong-Ri, S. Xin, H. Lin, F.-S. Zhang, *Chin. Phys. B* **2012**, *21*, 086402.
- [42] a) H.-L. Kee, C. Kirmaier, L.-H. Yu, P. Thamyongkit, W. J. Youngblood, M. E. Calder, L. Ramos, B. C. Noll, D. F. Bocian, W. R. Scheidt, R. R. Birge, J. S. Lindsey, D. Holtz, *J. Phys. Chem. B* **2005**, *109*, 20433–20443; b) J. Herbich, A. Kapturkiewicz, *J. Am. Chem. Soc.* **1998**, *120*, 1014–1029.
- [43] J. Dobkowski, P. Wnuk, J. Buczyńska, M. Pszona, G. Orzanowska, D. Frath, G. Ulrich, J. Massue, S. Mosquera-Vázquez, E. Vauthey, C. Radzewicz, R. Ziessel, J. Waluk, *Chem. Eur. J.* **2015**, *21*, 1312–1327.
- [44] E. Görlach, H. Gygax, P. Lubini, U. P. Wild, *Chem. Phys.* **1995**, *194*, 185–193.
- [45] J.-Z. Zhao, K.-J. Xu, W.-B. Yang, Z.-J. Wang, F.-F. Zhong, *Chem. Soc. Rev.* **2015**, *44*, 8904–8939.
- [46] L. Porrès, A. Holland, L.-O. Pålsson, A. P. Monkman, C. Kemp, A. Beeby, *J. Fluoresc.* **2006**, *16*, 267–272.
- [47] a) J.-T. He, B. Xu, F.-P. Chen, H.-J. Xia, K.-P. Li, L. Ye, W.-J. Tian, *J. Phys. Chem. C* **2009**, *113*, 9892–9899; b) F. Bu, R.-H. Duan, Y.-J. Xie, Y.-P. Yi, Q. Peng, R.-R. Hu, A.-J. Qin, Z.-J. Zhao, B.-Z. Tang, *Angew. Chem. Int. Ed.* **2015**, *54*, 14492–14497; *Angew. Chem.* **2015**, *127*, 14700–14705; c) T. Zhang, H.-L. Ma, Y.-L. Niu, W.-Q. Li, D. Wang, Q. Peng, Z.-G. Shuai, W.-Z. Liang, *J. Phys. Chem. C* **2015**, *119*, 5040–5047; d) S.-J. Liu, Y.-Y. Li, H.-K. Zhang, Z. Zhao, X.-F. Lu, J. W. Y. Lam, B.-Z. Tang, *ACS Mater. Lett.* **2019**, *1*, 425–429.

- [48] Z. Krumer, W. G. J. H. M. van Sark, R. E. I. Schropp, C. M. Donega, *Solar Ener. Mater. Solar Cells* **2017**, *167*, 133–139.
- [49] M. K. Bera, P. Pal, S. Malik, *J. Mater. Chem. C* **2020**, *8*, 788–802.
- [50] a) R. B. Alnoman, S. Rihn, D. C. O'Connor, F. A. Black, B. Costello, P. G. Waddell, W. Clegg, R. D. Peacock, W. Herrebout, J. G. Knight, M. J. Hall, *Chem. Eur. J.* **2016**, *22*, 93–96; b) R. I. Lerrick, T. P. L. Winstanley, K. Haggerty, C. Wills, W. C. Clegg, R. W. Harrington, P. Bultinck, W. Herrebout, A. C. Benniston, M. J. Hall, *Chem. Commun.* **2014**, *50*, 4714–4716.
- [51] B. Kozma, A. Tajti, B. Demoulin, R. Izsák, M. Nooijen, P. G. Szalay, *J. Chem. Theory Comput.* **2020**, *16*, 4213–4225.
- [52] S. Grimme, *J. Comput. Chem.* **2006**, *27*, 1787–1799.
- [53] L. Goerigk, J. Moellmann, S. Grimme, *Phys. Chem. Chem. Phys.* **2009**, *11*, 4611–4620.
- [54] J. Jiménez, J. Sánchez-Camacho, F. Moreno, A. R. Agarrabeitia, T. Arbeloa, T. A. Cabreros, G. Muller, J. Bañuelos, B. L. Maroto, S. de la Moya, *Proceedings* **2020**, *41*, 53.
- [55] a) Y. Wu, S. Wang, Z. Li, Z. Shen, H. Lu, *J. Mater. Chem. C* **2016**, *4*, 4668–4674; b) E. M. Sánchez-Carnerero, F. Moreno, B. L. Maroto, A. R. Agarrabeitia, M. J. Ortiz, B. G. Vo, G. Muller, S. de la Moya, *J. Am. Chem. Soc.* **2014**, *136*, 3346–3349; c) F. Zinna, T. Bruhn, C. A. Guido, J. Ahrens, M. Bröring, L. Di Bari, G. Pescitelli, *Chem. Eur. J.* **2016**, *22*, 16089–16098.
- [56] R. Sola-Llano, J. Jiménez, E. Avellanal-Zaballa, M. Johnson, T. A. Cabreros, F. Moreno, B. L. Maroto, G. Muller, J. Bañuelos, L. Cerdán, I. García-Moreno, S. de la Moya, *Dyes Pigm.* **2019**, *170*, 107662.
- [57] P. A. A. M. Vaz, J. Rocha, A. M. S. Silva, S. Guieu, *New J. Chem.* **2018**, *42*, 18166–18171.
- [58] Y. Hong, J. W. Y. Lam, B. Z. Tang, *Chem. Commun.* **2009**, 4332–4353.
- [59] R. C. Clark, J. S. Reid, *Acta Crystallogr. Sect. A* **1995**, *51*, 887–897.
- [60] CrysAlisPro, Rigaku Oxford Diffraction, Tokyo, Japan.
- [61] G. M. Sheldrick, *Acta Crystallogr. Sect. A* **2015**, *71*, 3–8.
- [62] G. M. Sheldrick, *Acta Crystallogr. Sect. A* **2008**, *64*, 112–122.
- [63] O. V. Dolomanov, L. J. Bourhis, R. J. Gildea, J. A. K. Howard, H. Puschmann, *J. Appl. Crystallogr.* **2009**, *42*, 339–341.
- [64] Gaussian 16, Revision A.03, M. J. Frisch, G. W. Trucks, H. B. Schlegel, G. E. Scuseria, M. A. Robb, J. R. Cheeseman, G. Scalmani, V. Barone, G. A. Petersson, H. Nakatsuji, X. Li, M. Caricato, A. V. Marenich, J. Bloino, B. G. Janesko, R. Gomperts, B. Mennucci, H. P. Hratchian, J. V. Ortiz, A. F. Izmaylov, J. L. Sonnenberg, D. Williams-Young, F. Ding, F. Lipparini, F. Egidi, J. Goings, B. Peng, A. Petrone, T. Henderson, D. Ranasinghe, V. G. Zakrzewski, J. Gao, N. Rega, G. Zheng, W. Liang, M. Hada, M. Ehara, K. Toyota, R. Fukuda, J. Hasegawa, M. Ishida, T. Nakajima, Y. Honda, O. Kitao, H. Nakai, T. Vreven, K. Throssell, J. A. Montgomery, Jr., J. E. Peralta, F. Ogliaro, M. J. Bearpark, J. J. Heyd, E. N. Brothers, K. N. Kudin, V. N. Staroverov, T. A. Keith, R. Kobayashi, J. Normand, K. Raghavachari, A. P. Rendell, J. C. Burant, S. S. Iyengar, J. Tomasi, M. Cossi, J. M. Millam, M. Klene, C. Adamo, R. Cammi, J. W. Ochterski, R. L. Martin, K. Morokuma, O. Farkas, J. B. Foresman, D. J. Fox, Gaussian, Inc., Wallingford CT, **2016**.
- [65] GaussView, Version 6, R. Dennington, T. A. Keith, J. M. Millam, Semichem Inc., Shawnee Mission, KS, **2016**.
- [66] A. M. Brouwer, *Pure Appl. Chem.* **2011**, *83*, 2213–2228.
- [67] R. Bonnett, D. J. McGarvey, A. Harriman, E. J. Land, T. G. Truscott, U. J. Winfield, *Photochem. Photobiol.* **1988**, *48*, 271–276.
- [68] R. S. Knox, H. van Amerongen, *J. Phys. Chem. B* **2002**, *106*, 5289–5293.

Manuscript received: December 8, 2020

Revised manuscript received: December 24, 2020

Accepted manuscript online: December 28, 2020

Version of record online: February 16, 2021